






## Evolution of superconductivity and charge density wave through Ta and Mo doping in CsV<sub>3</sub>Sb<sub>5</sub>

Mengqin Liu,<sup>1</sup> Tao Han <sup>1,2,\*</sup> Xinran Hu <sup>3</sup> Yubing Tu,<sup>1,2</sup> Zongyuan Zhang,<sup>1,2</sup> Mingsheng Long <sup>1,2</sup> Xingyuan Hou <sup>1,2</sup> Qingge Mu,<sup>1,2,†</sup> and Lei Shan <sup>1,2,‡</sup>

<sup>1</sup>Information Materials and Intelligent Sensing Laboratory of Anhui Province,

Institutes of Physical Science and Information Technology, Anhui University, Hefei 230601, China

<sup>2</sup>Key Laboratory of Structure and Functional Regulation of Hybrid Materials of Ministry of Education, Anhui University, Hefei 230601, China

<sup>3</sup>School of Physics and Optoelectronic Engineering, Anhui University, Hefei 230601, China



(Received 3 August 2022; revised 15 September 2022; accepted 22 September 2022; published 3 October 2022)

Here, we report the tuning study of superconductivity and charge density wave in CsV<sub>3</sub>Sb<sub>5</sub> through the V kagome net doping. Combining electrical transport and magnetic susceptibility measurements, we reveal the opposite effect of Ta and Mo doping. Ta doping promotes the superconductivity but suppresses charge density wave, which may be explained by the lift of van Hove singularity towards  $E_F$ . On the contrary, Mo doping suppresses the superconductivity quickly and leads to a continuous increase of charge density wave temperature up to 100.7 K. Our result suggests that electron doping can also effectively tune charge density wave state in CsV<sub>3</sub>Sb<sub>5</sub>.

DOI: [10.1103/PhysRevB.106.L140501](https://doi.org/10.1103/PhysRevB.106.L140501)

Owing to the corner-sharing triangle structure, the kagome lattice offers an ideal playground to study many quantum phenomena, such as frustrated magnetism [1,2], topological state [3–8], density wave [9], and unconventional superconductivity [9–12]. These phenomena mainly arise from the intrinsic flat bands, Dirac cones, and van Hove singularities across the Brillouin zone and deeply depend on the band filling.

Recently, the newly discovered kagome metals AV<sub>3</sub>Sb<sub>5</sub> (KV<sub>3</sub>Sb<sub>5</sub>, RbV<sub>3</sub>Sb<sub>5</sub>, CsV<sub>3</sub>Sb<sub>5</sub>) have drawn much interest due to the coexistence of superconductivity (SC), charge density wave (CDW), and nontrivial topological state [13–16]. The AV<sub>3</sub>Sb<sub>5</sub> show a layered structure of V-Sb sheets with the V atoms forming a kagome lattice, the alkali metal ion A was intercalated between the layers. Among them, CsV<sub>3</sub>Sb<sub>5</sub> shows the highest superconducting transition temperature. For CsV<sub>3</sub>Sb<sub>5</sub>, transport studies showed a superconducting transition temperature of about 2.7 K and charge density wave state at 94 K. Even though no magnetic order or local moment was detected by neutron scattering [15], a giant anomalous Hall effect [17] was observed in transport study and time-reversal symmetry-breaking signals below CDW order were observed by muon spin spectroscopy measurement [18], implying a hidden flux phase exists and may be connected with the CDW order [18,19]. Nuclear magnetic resonance and magnetic penetration depth measurements manifest nodeless superconductivity [20,21], while ultralow-temperature thermal conductivity measurements suggest nodal superconductivity [22]. Scanning tunneling microscopy/spectroscopy

observed the Majorana zero-energy mode excitation [23], pair density wave state [24], and nematic state [25], resembling unconventional superconductivity in CsV<sub>3</sub>Sb<sub>5</sub>. Pressure experiments showed a suppressed CDW transition and a double-domelike SC behavior, indicating an unusual competition between CDW and SC [26–29]. Recent studies on oxidized thin flakes of CsV<sub>3</sub>Sb<sub>5</sub> or CsTi<sub>x</sub>V<sub>3–x</sub>Sb<sub>5</sub> and CsV<sub>3</sub>Sb<sub>5–x</sub>Sn<sub>x</sub>—doped samples revealed that hole doping enhances superconducting temperature ( $T_c$ ) while it suppresses the CDW order [30–32], which was believed to be caused by the shift of van Hove singularities (VHS) towards  $E_F$  [33].

In this work, the doping effect of CsV<sub>3</sub>Sb<sub>5</sub> was studied by partial Ta or Mo substitution of V atoms in the kagome net. Electrical transport measurements show an obvious decrease of CDW transition temperature  $T_{CDW}$  from 93.5 to 66.7 K when V was replaced by Ta atoms partially, accompanied with a slight increase of superconducting temperature  $T_c$ . This is similar to some tuning results in CsV<sub>3</sub>Sb<sub>5</sub>, such as the exfoliation experiment [30] and Nb-doping results [34]. On the contrary, in the Mo-doping samples CsMo<sub>x</sub>V<sub>3–x</sub>Sb<sub>5</sub>, the CDW transition temperature  $T_{CDW}$  was increased from 93.5 to 100.7 K when the doping content  $x$  increased to 0.105, and the superconducting temperature was quickly suppressed to below 50 mK. This is a report of increased CDW transition temperature in this kagome superconductor through doping.

Several batches of CsA<sub>x</sub>V<sub>3–x</sub>Sb<sub>5</sub> (A = Ta, Mo) single crystal were synthesized via a flux method. Starting materials with a stoichiometric molar ratio (Cs:A + V:Sb) of 1:3:15 were mixed in an alumina crucible and then sealed in a quartz tube. The mixture was slowly heated to 1273 K and kept at this temperature for 24 h. Then, the quartz was slowly cooled to 1073 K at a rate of 2 K/h before it was

\*than@ahu.edu.cn

†mu@ahu.edu.cn

‡lshan@ahu.edu.cn

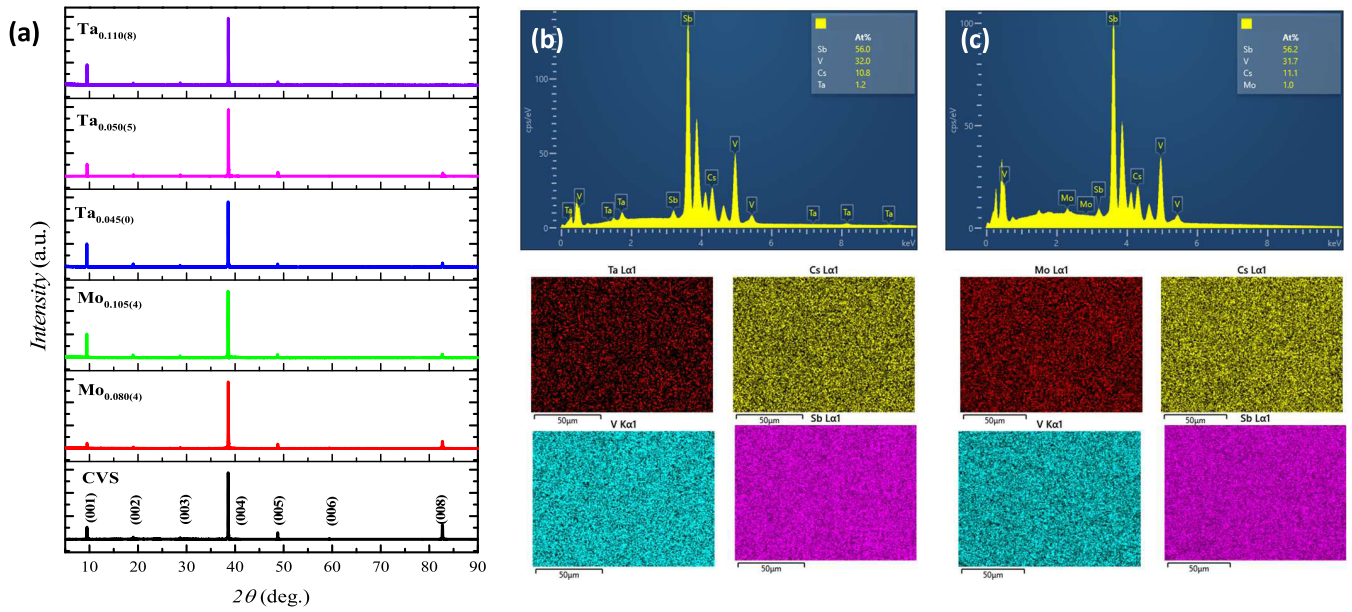


FIG. 1. Structure characterization and stoichiometric ratio of the  $\text{CsA}_x\text{V}_{3-x}\text{Sb}_5$  ( $A = \text{Ta}, \text{Mo}$ ) single crystals. (a) Typical XRD patterns of undoped CVS and several  $\text{CsA}_x\text{V}_{3-x}\text{Sb}_5$  ( $A = \text{Ta}, \text{Mo}$ ) single crystals. (b) EDS and mappings of  $\text{Cs}_{0.977(13)}\text{Ta}_{0.108(9)}\text{V}_{2.910(23)}\text{Sb}_{5.007(45)}$ . (c) EDS and mappings of  $\text{Cs}_{1.001(17)}\text{Mo}_{0.092(11)}\text{V}_{2.832(15)}\text{Sb}_{5.076(23)}$ .

centrifuged at a speed of 3000 r/min. After that, millimeter-sized platelike crystals were obtained. Phase purity and crystal quality were examined by x-ray diffraction (XRD) collected using a PANalytical Empyrean S3 with  $\text{Cu-K}\alpha 1$  radiation at room temperature. The chemical composition contents and the composition mappings were checked by a Zeiss cross-beam 550L system equipped with Oxford spectroscopy. Electrical transport measurements were performed on a Quantum Design Physical Property Measurement System (PPMS DynaCool), DC magnetic susceptibility was measured by a Quantum Design Magnetic Property Measurement System (MPMS3).

The characterization of  $\text{CsA}_x\text{V}_{3-x}\text{Sb}_5$  ( $A = \text{Ta}, \text{Mo}$ ) single crystals is shown in Fig. 1. Here, we took some doping contents as examples; in Fig. 1(a), six batches of XRD patterns of  $\text{CsV}_3\text{Sb}_5$  and  $\text{CsA}_x\text{V}_{3-x}\text{Sb}_5$  ( $A = \text{Ta}, \text{Mo}$ ) single crystals were displayed. All the XRD patterns show the same reflection, which can be indexed by the  $(00l)$  patterns of  $P6/mmm$ . The undoped  $\text{CsV}_3\text{Sb}_5$  single crystal and the two highest doping content of  $\text{CsTa}_x\text{V}_{3-x}\text{Sb}_5$  and  $\text{CsMo}_x\text{V}_{3-x}\text{Sb}_5$  were later ground into powders to get the full patterns to calculate the lattice parameters. The doping content and homogeneity of the doped samples were checked by energy-dispersive spectrometer (EDS). For each sample, we took at least 4–5 sites in different areas to get the average chemical compositions. Here, for the lowest Mo-doping sample, the doping content is too small to get an accurate value from the EDS data. So, we carried out the inductively coupled plasma atomic emission spectroscopy (ICP-AES) measurement and the doping composition was determined to be  $\text{Mo}_{0.007(1)}$  from the ICP results. More details are available in the Supplemental Material [35]. The Ta peaks and Mo peaks were observed in all the  $\text{CsTa}_x\text{V}_{3-x}\text{Sb}_5$  and  $\text{CsMo}_x\text{V}_{3-x}\text{Sb}_5$  samples. In the periodic table, Ta and V belongs to the same main group, while Mo sits near the V site, which are all far away from the Cs and Sb

positions. The similar physical and chemical properties suggest the possibility of Ta and Mo substitution at the V sites in the kagome lattice, which were confirmed by our EDS results. As shown in Fig. 1(b) and Fig. 1(c), the doping content of two typical Ta- and Mo-doped single crystals were determined to be  $\text{Cs}_{0.977(13)}\text{Ta}_{0.108(9)}\text{V}_{2.910(23)}\text{Sb}_{5.007(45)}$  and  $\text{Cs}_{1.001(17)}\text{Mo}_{0.092(11)}\text{V}_{2.832(15)}\text{Sb}_{5.076(23)}$ , respectively; more details are available in the Supplemental Material [35]. The EDS mappings shown below indicate the doping content of Ta/Mo atoms were uniformly distributed in the single crystal. In our paper, all the doping contents were using the real-content  $x$  from EDS results instead of the nominal ones.

Temperature-dependent resistivity of  $\text{CsA}_x\text{V}_{3-x}\text{Sb}_5$  ( $A = \text{Ta}, \text{Mo}$ ) single crystals were measured with the temperature ranging from 2 to 300 K. As shown in Fig. 2(a), all the  $\text{CsTa}_x\text{V}_{3-x}\text{Sb}_5$  single crystals with the highest doping-content  $x$  reaching to 0.134 show superconducting transition below 3.5 K. Also, the anomaly below 94 K indicating the CDW transition was clearly observed in all the Ta-doped samples and the anomaly was gradually moved to lower temperature as the doping-content  $x$  increases. To precisely determine the CDW transition temperature  $T_{\text{CDW}}$ , the derivative of resistivity curves is displayed in Fig. 2(b). Interestingly, the CDW behavior was transformed from a kinklike resistivity anomaly to a humplike resistivity anomaly upon doping, resulting in a change of peak with maximum value to valley with minimum value in the derived resistivity curves, just like the case in the high-pressure study [26,28]. So, here the maximum values and minimum values were used to determine the CDW transition temperature for the kinklike anomaly and humplike anomaly, respectively.  $T_{\text{CDW}}$  of undoped  $\text{CsV}_3\text{Sb}_5$  was determined to be 93.5 K, which is a little lower than the early studies of 94 K. As the Ta-doping content increases, the  $T_{\text{CDW}}$  decreases monotonically to 66.7 K for  $\text{Ta}_{0.134(10)}$  sample. Meanwhile, a slight enhancement of superconduct-

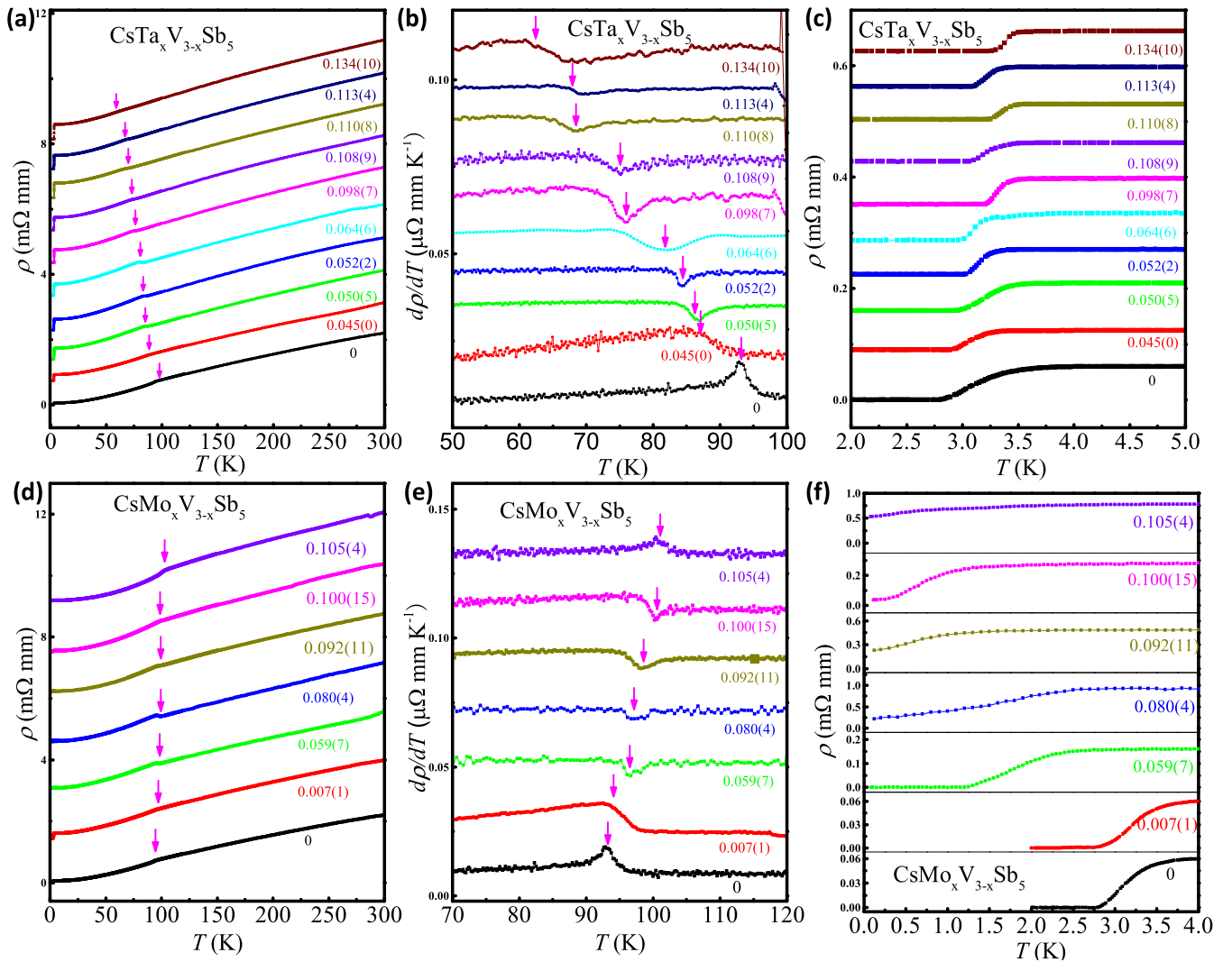


FIG. 2. Electrical transport measurements of the  $\text{CsA}_x\text{V}_{3-x}\text{Sb}_5$  ( $A = \text{Ta}, \text{Mo}$ ) single crystals. (a) Temperature-dependent resistivity of  $\text{CsTa}_x\text{V}_{3-x}\text{Sb}_5$  single crystals measured from 2 to 300 K. (b) The derivative of (a) from 50 to 100 K. Magenta arrows indicate the CDW transition temperature  $T_{\text{CDW}}$ . (c) Zoomed-in resistivity curves of  $\text{CsTa}_x\text{V}_{3-x}\text{Sb}_5$  around the superconducting transition. (d) Temperature-dependent resistivity of  $\text{CsMo}_x\text{V}_{3-x}\text{Sb}_5$  single crystals measured from 2 to 300 K. (e) The derivative of (d) from 70 to 120 K. Magenta arrows indicate the CDW transition temperature  $T_{\text{CDW}}$ . (f) Zoomed-in resistivity curves of  $\text{CsMo}_x\text{V}_{3-x}\text{Sb}_5$  around the superconducting transition.

tivity was observed; the superconducting temperature of zero resistivity  $T_{\text{c(zer0)}}$  was increased from 2.78 K for  $\text{CsV}_3\text{Sb}_5$  to 3.23 K for  $\text{Ta}_{0.134(10)}$  sample. On the contrary, the superconducting transition temperature decreased rapidly when a small amount of Mo atoms were doped in the  $\text{CsMo}_x\text{V}_{3-x}\text{Sb}_5$  single crystals. As shown in Fig. 2(d), when the doping-content  $x$  reaches to 0.059, no zero resistivity was observed above 2 K. To further define the superconducting transition temperature in high doping contents, ultralow-temperature electrical transport studies down to 50 mK were measured using the Dynacool equipped dilution refrigerator. The superconducting temperature with zero resistivity of  $\text{Mo}_{0.059(7)}$  sample was reduced to 1.3 K. Furthermore, for higher doping contents, a decreased onset superconducting temperature was observed and no zero resistivity was reached down to 50 mK, together with an increased superconducting transition width. All these evidenced the negative effect of superconductivity upon Mo doping. The CDW transition temperature obtained from the

derived resistivity curves in Fig. 2(e) gradually increases with the increasing of Mo doping content, and reaches to about 100.7 K with the highest doping content of 0.105. This is a report that doping can enhance CDW transition temperature in this kagome superconductor.

To further confirm the evolution of superconductivity and charge density wave, temperature-dependent magnetic susceptibility was measured with the applied field parallel to the  $ab$  plane. The superconducting transition temperature and CDW transition temperature were measured under a magnetic field of 10 Oe and 1 T, respectively. As shown in Fig. 3(a), the MT curves of several batches of  $\text{CsTa}_x\text{V}_{3-x}\text{Sb}_5$  single crystals show a slightly increased superconducting transition temperature from 2.55 K for  $\text{CsV}_3\text{Sb}_5$  to 3.15 K for the  $\text{Ta}_{0.110(8)}$  sample, and then the diamagnetic temperature decreased to 3.1 K for the  $\text{Ta}_{0.134(10)}$  sample. The change of CDW transition can be identified through the inflection point in MT curves shown in Fig. 3(b), which were all measured in zero-field

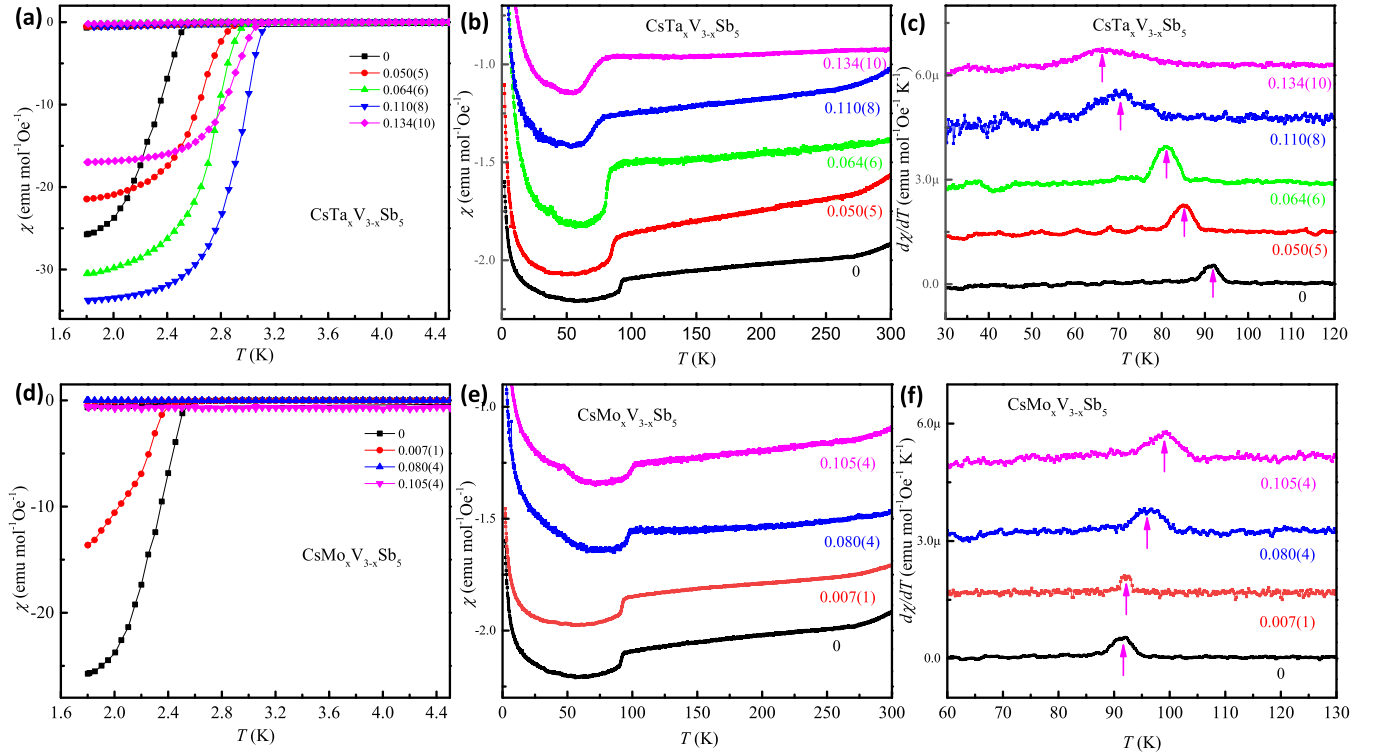


FIG. 3. Magnetic measurements of the  $\text{CsA}_x\text{V}_{3-x}\text{Sb}_5$  ( $A = \text{Ta}, \text{Mo}$ ) single crystals. (a) Temperature-dependent magnetic susceptibility of  $\text{CsTa}_x\text{V}_{3-x}\text{Sb}_5$  single crystals measured with the applied field of 10 Oe; both zero-field cooling (ZFC) and field-cooling (FC) curves were presented. (b) ZFC curves of  $\text{CsTa}_x\text{V}_{3-x}\text{Sb}_5$  single crystals measured with the applied field of 1 T. (c) The derivative of (b) from 30 to 120 K. Magenta arrows indicate the CDW transition temperature  $T_{\text{CDW}}$ . (d) Temperature-dependent magnetic susceptibility of  $\text{CsMo}_x\text{V}_{3-x}\text{Sb}_5$  single crystals measured with the applied field of 10 Oe; both ZFC and FC curves were presented. (e) ZFC curves of  $\text{CsMo}_x\text{V}_{3-x}\text{Sb}_5$  single crystals measured with the applied field of 1 T. (f) The derivative of (e) from 60 to 130 K. Magenta arrows indicate the CDW transition temperature  $T_{\text{CDW}}$ .

cooling mode with the applied field of 1 T. The derivative of magnetic susceptibility shown in Fig. 3(c) shows a decreased CDW transition temperature upon Ta doping; the  $T_{\text{CDW}}$  defined by the peak of derivative curves decreases from 92 K for  $\text{CsV}_3\text{Sb}_5$  to 66 K for the  $\text{Ta}_{0.134(10)}$  sample.

While for the Mo-doping samples, the superconductivity was suppressed quickly. Here, we also measured the magnetic susceptibility for some typical Mo-doped samples, together with an undoped  $\text{CsV}_3\text{Sb}_5$  single crystal. As shown in Fig. 3(d), upon doping,  $T_c$  decreases gradually from 2.55 to 2.45 K for the  $\text{Mo}_{0.009(0)}$  sample. Moreover, two  $\text{CsMo}_x\text{V}_{3-x}\text{Sb}_5$  samples ( $x = 0.08, 0.105$ ) show no superconducting diamagnetic signal above 1.8 K. The inflection point of  $\chi-T$  curves in Fig. 3(e) and peak of  $d\chi/dT$  curves in Fig. 3(f) confirmed the enhanced CDW transition temperature. The observed  $T_{\text{CDW}}$  here determined by the magnetic susceptibility seems to be a little lower than that in transport measurements.

Figure 4 summarizes the effects of Ta and Mo doping on both the superconductivity and CDW orders from the transport measurements. Here, the  $T_{c(\text{zero})}$  and  $T_{c(\text{mid})}$  were defined as the temperature where the drop of resistivity reaches 0 and 50% of the normal resistivity at 5 K, respectively. Ta doping results in a continuously decreased CDW temperature and slightly increased superconducting transition temperature. Similar to the Nb-doping effect [34], the CDW and

superconductivity coexist in the whole doping range. This is different from the  $\text{CsTi}_x\text{V}_{3-x}\text{Sb}_5$  and  $\text{CsV}_3\text{Sb}_{5-x}\text{Sn}_x$  systems and the high-pressure experiments [26,31,32], which show a fully suppressed CDW state and two dome superconducting regions, while for the Mo-doping phase diagram, the zero-resistivity superconducting temperature was fully suppressed when the doping content reached to 0.08, accompanied with the CDW transition temperature  $T_{\text{CDW}}$  increased to 97 K. Moreover  $T_{\text{CDW}}$  was enhanced to 100.7 K when the Mo doping-content  $x$  reaches to 0.105. We attempted to grow higher doping samples but failed; the residual resistivity ratio (RRR) of the highest doping content in our experiment is about 5, which is higher or comparable to other doping reports [31,32]. The opposite evolution of charge density wave and superconductivity in both the Ta- and Mo-doping experiments reveals the competition between these two quantum states in  $\text{CsV}_3\text{Sb}_5$ .

Early studies suggest the V-based kagome net plays an important role in the fertile quantum states of  $\text{CsV}_3\text{Sb}_5$ . Hole doping lifts the van Hove singularity (VHS) up to the Fermi level and results in an increase in density of states (DOS) at  $E_F$ , which was considered to be responsible for the enhanced superconductivity [30,32,33]. For the Nb-doped samples [34], the enlarged lattice parameter  $a$  results in a lift of VHS near the  $M$  points and breaks the multiband behavior, which turns to an increased DOS at  $E_F$  and a reduced nesting

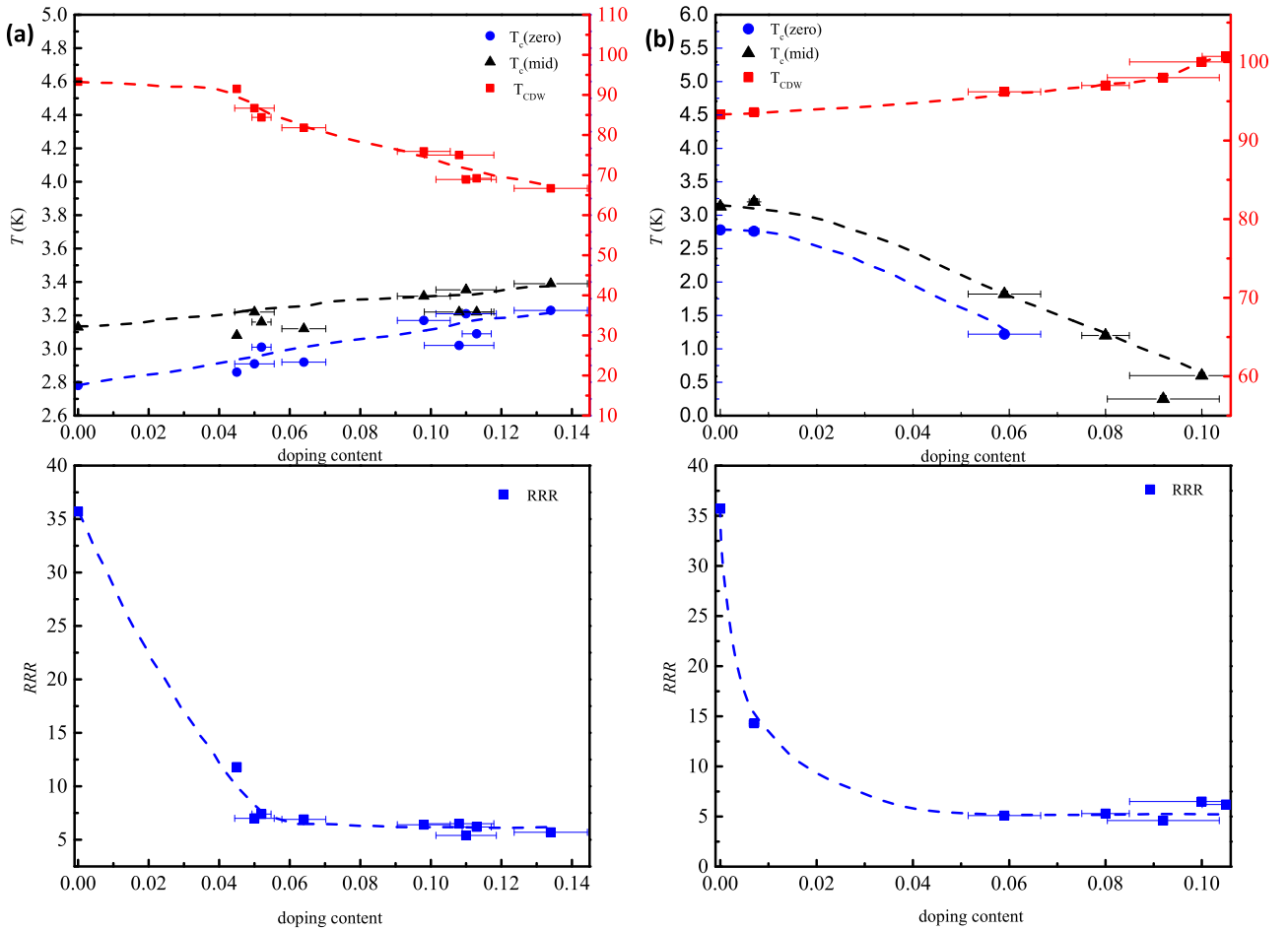


FIG. 4. Phase diagram of the  $\text{CsA}_x\text{V}_{3-x}\text{Sb}_5$  ( $A = \text{Ta}, \text{Mo}$ ) single crystals; all the data were based on the electrical transport measurements. (a) Evolution of CDW and superconductivity upon Ta doping; lower plot presents the change of RRR. (b) Evolution of CDW and superconductivity upon Mo doping; lower plot presents the change of RRR.

effect at the Fermi surface. This explains why Nb doping increases the superconducting temperature and reduces the CDW temperature. In our experiment, the lattice parameters of the  $\text{Ta}_{0.134(10)}$  sample and  $\text{Mo}_{0.105(4)}$  sample were estimated through powder XRD patterns. Ta doping results in a similar structural change of Nb-doped samples; the lattice parameter  $a$  increases to  $5.5075 \text{ \AA}$  and  $c$  remains almost the same ( $9.3078 \text{ \AA}$ ) for the  $\text{Ta}_{0.134(10)}$  sample. So, we suppose the scenario of doping-induced enhancement of DOS at  $E_F$  and reduction of Fermi-surface nesting effect is suitable in our Ta-doping results. Doping or pressure induced the emergence or enhancement of superconductivity and the suppression of CDW order were also reported in some transition-metal dichalcogenides [36–42].

Now we turn to the Mo-doping results. Mo ionic diameter ( $0.65 \text{ \AA}$ ) is sizable compared to Ta ionic diameter ( $0.64 \text{ \AA}$ ), which are all larger than the substituted V ionic diameter ( $0.59 \text{ \AA}$ ). This results in an enlarged lattice parameter of both  $a$  and  $c$ . For the  $\text{Mo}_{0.105(4)}$  sample, the lattice parameter was calculated to be  $5.5051$  and  $9.3339 \text{ \AA}$  for  $a$  and  $c$ , respectively, both larger than the  $\text{CsV}_3\text{Sb}_5$  sample ( $a = 5.4945 \text{ \AA}$ ,  $c = 9.3101 \text{ \AA}$ ). The uniaxial strain and pressure results sug-

gest that the  $c$ -axis lattice parameter is the dominant structure parameter that controls the tuning of CDW and superconductivity [43]. In the strain study, the  $T_{\text{CDW}}$  was finally increased to  $97.5 \text{ K}$  when the applied compressive strain introduced an enlarged  $c$  of about  $0.35\%$ . In our  $\text{CsMo}_{0.105}\text{V}_{2.895}\text{Sb}_5$  sample, the estimated  $(c - c_0)/c_0$  was about  $0.25\%$ , which was smaller than the largest compressive uniaxial strain (about  $0.35\%$ ). On the other hand, the  $T_{\text{CDW}}$  in the  $\text{Mo}_{0.105(4)}$  sample was  $100.7 \text{ K}$ , larger than that in the terminal compressive uniaxial strain ( $97.5 \text{ K}$ ). So, the enhancement of  $T_{\text{CDW}}$  in our Mo-doping samples cannot only be explained by the increased  $c$ -lattice parameter. Moreover, unlike the Nb and Ta doping, Mo doping introduces electrons; the introduced electron carriers may play a positive role in the enhanced CDW order. Whether the increased  $c$ -lattice parameter and introduced electron carriers contribute to the enhancement of CDW order and suppression of superconductivity can be further studied by ion intercalation or ionic liquid-gating experiments.

In summary, we have studied the evolution of charge density wave and superconductivity in the fantastic kagome superconductor  $\text{CsV}_3\text{Sb}_5$  through Ta and Mo doping. CDW temperature was suppressed with the increasing doping

content of Ta, together with a slight increase of superconducting temperature. On the contrary, Mo doping results in a continuous increase of CDW temperature and reduction of superconductivity. The  $T_{CDW}$  in  $\text{Mo}_{0.105(4)}$  sample was increased to 100.7 K, which shows that doping can enhance  $T_{CDW}$  in  $\text{CsV}_3\text{Sb}_5$ . We hope the competing evolution and different scenario revealed in our work can provide a platform to study the fundamental physics of diverse quantum states in the kagome superconductors.

We thank Prof. Y. Y. Wang for helpful discussion. This work was supported by the National Nature Science Foundation of China (Grant No. 12074002), National Key R&D Program of China (Grants No. 2018YFA0305602 and No. 2017YFA0302904), and Key Project of Natural Scientific Research of Universities in Anhui Province (Grant No. K120462023).

M.Q.L. and T.H. contributed equally to this work.

The authors declare no competing financial interest.

- 
- [1] L. Balents, *Nature (London)* **464**, 199 (2010).
- [2] F. Pollmann, P. Fulde, and K. Shtengel, *Phys. Rev. Lett.* **100**, 136404 (2008).
- [3] H. M. Guo and M. Franz, *Phys. Rev. B* **80**, 113102 (2009).
- [4] M. Kang, S. Fang, L. Ye, H. C. Po, J. Denlinger, C. Jozwiak, A. Bostwick, E. Rotenberg, E. Kaxiras, J. G. Checkelsky, and R. Comin, *Nat. Commun.* **11**, 4004 (2020).
- [5] Z. Liu, M. Li, Q. Wang, G. Wang, C. Wen, K. Jiang, X. Lu, S. Yan, Y. Huang, D. Shen, J. X. Yin, Z. Wang, Z. Yin, H. Lei, and S. Wang, *Nat. Commun.* **11**, 4002 (2020).
- [6] E. Liu, Y. Sun, N. Kumar, L. Muchler, A. Sun, L. Jiao, S. Y. Yang, D. Liu, A. Liang, Q. Xu, J. Kroder, V. Suss, H. Borrmann, C. Shekhar, Z. Wang, C. Xi, W. Wang, W. Schnelle, S. Wirth, Y. Chen, S. T. B. Goennenwein, and C. Felser, *Nat. Phys.* **14**, 1125 (2018).
- [7] M. Kang, L. Ye, S. Fang, J. S. You, A. Levitan, M. Han, J. I. Facio, C. Jozwiak, A. Bostwick, E. Rotenberg, M. K. Chan, R. D. McDonald, D. Graf, K. Kaznatcheev, E. Vescovo, D. C. Bell, E. Kaxiras, J. van den Brink, M. Richter, M. Prasad Ghimire, J. G. Checkelsky, and R. Comin, *Nat. Mater.* **19**, 163 (2020).
- [8] N. Morali, R. Batabyal, P. K. Nag, E. Liu, Q. Xu, Y. Sun, B. Yan, C. Felser, N. Avraham, and H. Beidenkopf, *Science* **365**, 1286 (2019).
- [9] S.-L. Yu and J.-X. Li, *Phys. Rev. B* **85**, 144402 (2012).
- [10] M. L. Kiesel, C. Platt, and R. Thomale, *Phys. Rev. Lett.* **110**, 126405 (2013).
- [11] C. Mielke, Y. Qin, J. X. Yin, H. Nakamura, D. Das, K. Guo, R. Khasanov, J. Chang, Z. Q. Wang, S. Jia, S. Nakatsuji, A. Amato, H. Luetkens, G. Xu, M. Z. Hasan, and Z. Guguchia, *Phys. Rev. Mater.* **5**, 034803 (2021).
- [12] W.-S. Wang, Z.-Z. Li, Y.-Y. Xiang, and Q.-H. Wang, *Phys. Rev. B* **87**, 115135 (2013).
- [13] Y. Fu, N. Zhao, Z. Chen, Q. Yin, Z. Tu, C. Gong, C. Xi, X. Zhu, Y. Sun, K. Liu, and H. Lei, *Phys. Rev. Lett.* **127**, 207002 (2021).
- [14] Y. Hu, S. M. Teicher, B. R. Ortiz, Y. Luo, S. Peng, L. Huai, J. Ma, N. Plumb, S. D. Wilson, and J.-F. He, *Sci. Bull.* **67**, 495 (2022).
- [15] B. R. Ortiz, L. C. Gomes, J. R. Morey, M. Winiarski, M. Bordelon, J. S. Mangum, I. W. H. Oswald, J. A. Rodriguez-Rivera, J. R. Neilson, S. D. Wilson, E. Ertekin, T. M. McQueen, and E. S. Toberer, *Phys. Rev. Mater.* **3**, 094407 (2019).
- [16] B. R. Ortiz, S. M. L. Teicher, Y. Hu, J. L. Zuo, P. M. Sarte, E. C. Schueller, A. M. Milinda Abeykoon, M. J. Krogstad, S. Rosenkranz, R. Osborn, R. Seshadri, L. Balents, J. He, and S. D. Wilson, *Phys. Rev. Lett.* **125**, 247002 (2020).
- [17] F. H. Yu, T. Wu, Z. Y. Wang, B. Lei, W. Z. Zhuo, J. J. Ying, and X. H. Chen, *Phys. Rev. B* **104**, L041103 (2021).
- [18] C. W. L. Yu, Y. Zhang, M. Sander, S. Ni, Z. Lu, S. Ma, Z. Z. Wang, H. Chen *et al.*, [arXiv:2107.10714](https://arxiv.org/abs/2107.10714).
- [19] X. Feng, K. Jiang, Z. Wang, and J. Hu, *Sci. Bull.* **66**, 1384 (2021).
- [20] C. Mu, Q. Yin, Z. Tu, C. Gong, H. Lei, Z. Li, and J. Luo, *Chin. Phys. Lett.* **38**, 077402 (2021).
- [21] W. Duan, Z. Nie, S. Luo, F. Yu, B. R. Ortiz, L. Yin, H. Su, F. Du, A. Wang, Y. Chen, X. Lu, J. Ying, S. D. Wilson, X. Chen, Y. Song, and H. Yuan, *Sci. China-Phys. Mech. Astron.* **64**, 107462 (2021).
- [22] L. S. W. C. C. Zhao, W. Xia, Q. W. Yin, J. M. Ni, Y. Y. Huang, C. P. Tu, Z. C. Tao, Z. J. Tu, C. S. Gong, H. C. Lei, Y. F. Guo, X. F. Yang, and S. Y. Li, [arXiv:2102.08356](https://arxiv.org/abs/2102.08356).
- [23] Z. Liang, X. Hou, F. Zhang, W. Ma, P. Wu, Z. Zhang, F. Yu, J. J. Ying, K. Jiang, L. Shan, Z. Wang, and X. H. Chen, *Phys. Rev. X* **11**, 031026 (2021).
- [24] H. Chen, H. Yang, B. Hu, Z. Zhao, J. Yuan, Y. Xing, G. Qian, Z. Huang, G. Li, Y. Ye, S. Ma, S. Ni, H. Zhang, Q. Yin, C. Gong, Z. Tu, H. Lei, H. Tan, S. Zhou, C. Shen, X. Dong, B. Yan, Z. Wang, and H. J. Gao, *Nature (London)* **599**, 222 (2021).
- [25] L. Nie, K. Sun, W. Ma, D. Song, L. Zheng, Z. Liang, P. Wu, F. Yu, J. Li, M. Shan, D. Zhao, S. Li, B. Kang, Z. Wu, Y. Zhou, K. Liu, Z. Xiang, J. Ying, Z. Wang, T. Wu, and X. Chen, *Nature (London)* **604**, 59 (2022).
- [26] F. H. Yu, D. H. Ma, W. Z. Zhuo, S. Q. Liu, X. K. Wen, B. Lei, J. J. Ying, and X. H. Chen, *Nat. Commun.* **12**, 3645 (2021).
- [27] Z. Zhang, Z. Chen, Y. Zhou, Y. Yuan, S. Wang, J. Wang, H. Yang, C. An, L. Zhang, X. Zhu, Y. Zhou, X. Chen, J. Zhou, and Z. Yang, *Phys. Rev. B* **103**, 224513 (2021).
- [28] K. Y. Chen, N. N. Wang, Q. W. Yin, Y. H. Gu, K. Jiang, Z. J. Tu, C. S. Gong, Y. Uwatoko, J. P. Sun, H. C. Lei, J. P. Hu, and J. G. Cheng, *Phys. Rev. Lett.* **126**, 247001 (2021).
- [29] Q. Wang, P. Kong, W. Shi, C. Pei, C. Wen, L. Gao, Y. Zhao, Q. Yin, Y. Wu, G. Li, H. Lei, J. Li, Y. Chen, S. Yan, and Y. Qi, *Adv. Mater.* **33**, 2102813 (2021).
- [30] Y. Song, T. Ying, X. Chen, X. Han, X. Wu, A. P. Schnyder, Y. Huang, J. G. Guo, and X. Chen, *Phys. Rev. Lett.* **127**, 237001 (2021).
- [31] S. M. Z. Wang, Y. Zhang, H. Yang, Z. Zhao, Y. Ou, Y. Zhu, S. Ni, Z. Lu, H. Chen, K. Jiang, L. Yu, Y. Zhang, X. Dong, J. Hu, H. J. Gao, and Z. Zhao, [arXiv:2104.05556](https://arxiv.org/abs/2104.05556).
- [32] Y. M. Oey, B. R. Ortiz, F. Kaboudvand, J. Frassinetti, E. Garcia, R. Cong, S. Sanna, V. F. Mitrović, R. Seshadri, and S. D. Wilson, *Phys. Rev. Mater.* **6**, L041801 (2022).
- [33] H. LaBollita and A. S. Botana, *Phys. Rev. B* **104**, 205129 (2021).

- [34] Y. Li, Q. Li, X. Fan, J. Liu, Q. Feng, M. Liu, C. Wang, J.-X. Yin, J. Duan, X. Li, Z. Wang, H.-H. Wen, and Y. Yao, *Phys. Rev. B* **105**, L180507 (2022).
- [35] See Supplemental Material at <http://link.aps.org/supplemental/10.1103/PhysRevB.106.L140501> for details of some EDS results, XRD results, accurate chemical compositions, and the comparisons of two transport anomalies.
- [36] E. Morosan, H. W. Zandbergen, B. S. Dennis, J. W. G. Bos, Y. Onose, T. Klimczuk, A. P. Ramirez, N. P. Ong, and R. J. Cava, *Nat. Phys.* **2**, 544 (2006).
- [37] A. F. Kusmartseva, B. Sipos, H. Berger, L. Forro, and E. Tutiš, *Phys. Rev. Lett.* **103**, 236401 (2009).
- [38] M. Boubeche, N. Wang, J. Sun, P. Yang, L. Zeng, S. Luo, Y. He, J. Yu, M. Wang, J. Cheng, and H. Luo, *J. Phys.: Condens. Matter.* **34**, 205602 (2022).
- [39] L. Zeng, X. Hu, N. Wang, J. Sun, P. Yang, M. Boubeche, S. Luo, Y. He, J. Cheng, D. X. Yao, and H. Luo, *J. Phys. Chem. Lett.* **13**, 2442 (2022).
- [40] L. Zeng, Y. Ji, D. Yu, S. Guo, Y. He, K. Li, Y. Huang, C. Zhang, P. Yu, S. Luo, H. Wang, and H. Luo, *J. Phys. Chem. C* **126**, 3705 (2022).
- [41] J. Guo, C. Huang, H. Luo, H. Yang, L. Wei, S. Cai, Y. Zhou, H. Zhao, X. Li, Y. Li, K. Yang, A. Li, P. Sun, J. Li, Q. Wu, R. J. Cava, and L. Sun, *Phys. Rev. Mater.* **6**, L051801 (2022).
- [42] H. Liu, S. Huangfu, X. Zhang, H. Lin, and A. Schilling, *Phys. Rev. B* **104**, 064511 (2021).
- [43] T. Qian, M. H. Christensen, C. Hu, A. Saha, B. M. Andersen, R. M. Fernandes, T. Birol, and N. Ni, *Phys. Rev. B* **104**, 144506 (2021).